General Frequency Control with Aggregated Control Reserve Capacity from Time-Varying Sources: The Case of PHEVs

Andreas Ulbig, Matthias D. Galus, Spyros Chatzivasileiadis and Göran Andersson
ETH Zurich, EEH - Power Systems Laboratory
Physikstrasse 3, 8092 Zurich, Switzerland
E-mail: {ulbig, galus, spyros, andersson}@eeh.ee.ethz.ch

Abstract

Herein, the concept of an ancillary service manager is developed for the provision of additional control reserve capacity. The aggregating entity clusters time-varying, aggregated battery capacity from plug-in hybrid electric vehicle (PHEV) fleets and power reserves from conventional generators. It is shown that providing additional control reserve capacity from time-varying sources such as PHEVs is possible and beneficial for power system control.
An MPC framework is used as the algorithm of choice for the ancillary service manager. It is able to manage and allocate control reserve power efficiently from its sources, taking into account their constraints on available power, energy and ramping capabilities. The proposed method is applied to the IEEE 14 bus system featuring conventional generation units and several PHEV fleets with different charging patterns and availability profiles. Emergency situations, resulting in frequency deviations on different time-scales, are simulated. The MPC scheme proves to stabilise the grid frequency at all times taking into account the various parameter constraints of the different control sources.

I. Introduction

Recently, the concept of aggregators has been proposed for the aggregation of small, controllable distributed generators and loads in order to perform various services for power systems. Especially in the case of plug-in hybrid electric vehicles (PHEVs), ancillary services [1] are an attractive option as these services prove to be profitable [2]. However, such small energy storage units cannot contribute easily to procuring the services, as the power capacity of individual PHEVs is too small. Hence, the concept of aggregators, clustering large number of small units, PHEVs, controllable loads or generators, has been suggested [3]. Such schemes seem promising to balance fluctuating renewable power in-feeds [4].
Herein, an ancillary service management method is presented, which is able to aggregate conventional ancillary power sources, i.e. conventional generators, and time-variant, partially dispatchable sources such as aggregated battery capacity of PHEV fleets, wind farms or demand-side management (DSM) schemes. In the following, only the contribution of PHEVs is considered. The aggregator allocates and, in case of an ancillary service call, dispatches available control reserves according to their actual time variant power and energy constraints. From here on these sources are called time variant sources. The approach takes advantage of the complementary nature of the different power sources and results in a larger available control reserve capacity than if only regarding conventional, fully dispatchable sources.
Additional control reserve capacity offers the possibility to increase the transmission grid's stability reserve margins, meaning its capability to robustly respond to occurring fault events. Larger control reserve capacities can facilitate the integration of increasing amounts of fluctuating electric power in-feed from renewable energy sources (RES). Unfortunately, existing allocation frameworks for ancillary services, i.e. primary, secondary and tertiary control reserve, are rather rigid. Strict conditions apply for ancillary services [1] and potentially usable control reserve power from time-variant sources can hardly be employed.
An MPC scheme is proposed, which enables an optimal aggregation and grid frequency control via the dispatch of control reserve power from time-variant and conventional sources. The MPC scheme, differing from well-known ancillary service provision schemes, offers fault control on different time-scales. The control scheme is tested on an IEEE 14 bus, which is exposed to generator faults. Conventional generation units are used as the principal control actuator for general frequency control. Additional control reserve capacity is provided by the aggregation of several PHEV fleets. The fleets feature vehicles with different battery sizes, temporal behavior and hence different availability profiles.
The individual temporal PHEV behavior and energy demand are simulated with a simple vehicle model utilising realistic drive cycles, representing different driving patterns and distances [5]. The simulation and the subsequent clustering of individual PHEV trips manifests itself in an aggregated PHEV availability profile featuring different callable powers for charging and discharging and time-variant state of charges (SOCs) of the different fleets.
The remainder of the article is structured as follows: Section II presents a classification of conventional grid frequency control schemes. The benefits of having supplementary control reserve capacity, although time-variant, at ones disposal are discussed in Section III. The general framework of the ancillary service manager is presented in Section IV, while details on the employed MPC setup are explained in Section V. The simulation and aggregation of individual PHEVs for control purposes is discussed in Section VI. The benchmark transmission grid used as study model is explained in detail in Section VII, simulation setup and respective results are presented in Section VIII. Conclusions and an outlook on future work are given in Sections IX and X, respectively.

978-1-4244-7467-7/10/$26.00

II. Classification of Traditional Grid Frequency Regulation

Traditional grid frequency regulation is accomplished by conventional generation and storage units and carried out within the control zone concept. Control zones are typically but not necessarily countries where the transmission system operator (TSO) is in charge of procuring system security and regulation services [6]. Regulation can be divided into four categories.
For the first category the the damping effect can be considered. It is due to the inertia of the rotating masses of the generation units and can be considered to react instantaneously in all control zones. It is a purely physically-motivated effect and cannot be considered as an active control measure.
Primary control can be ranked in the second category. It is activated in all control zones and delivers an automated active power contribution. Primary control is normally realised through a static P controller.
Secondary control can be classified third, takes over primary and also delivers an automated active power contribution. It is normally realised through a static PI controller and only active in the control zone, where the power imbalance, i.e. the fault, occurred.
Finally, tertiary control, which is a manually implemented active power dispatch, can be scheduled as ancillary service for frequency stabilization. The classification is depicted in Fig. 1. The mathematical representation of these four categories can be formulated as:

$$\begin{aligned} P_{inertia} &= K_{inertia}\,\Delta\dot{f} \\ P_{primary} &= K_{primary}\,\Delta f \\ P_{secondary,j} &= -y_{primary} + d_{CR_j}^{T} u \\ P_{tertiary,j} &= -y_{secondary,j} \end{aligned} \qquad (1)$$

$$\forall j = 1, \ldots, n,$$

where, $P_{inertia}$ is the immediate power in-feed from the kinetic energy stored in the rotating mass of the generators in case of a frequency drop. $P_{primary}$ is the power in-feed to the grid from primary frequency control. According to the grid codes of the ENTSO-E Central Europe region, its required reaction time-frame is 5 to 30 sec. after a fault event [7]. $P_{secondary,j}$ corresponds to the power in-feed to the grid from secondary frequency control. It alleviates the effort of primary control reserve coming from generators of all n control regions of the grid by control reserve power u coming only from the control region CR_j, where a fault occurred. The required reaction time-frame is 30 sec. to 15 min. $P_{tertiary,j}$ corresponds to the power input to the grid from tertiary frequency control and is aimed at alleviating the effort of secondary control reserves. The required reaction time-frame is from 15 min. to several hours. The grid control structure is depicted in Fig. 2.
It is conceivable that in the future the traditional distinction between primary, secondary and tertiary control reserve power may eventually be modified due to changing general conditions of power system structures. With increasing in-feed of fluctuating energy sources and therefor changing requirements on reaction times and procurable amounts as well as increasingly available computational power, the emergence of new grid control schemes is plausible. One possibility would be to merge the overlapping control tasks of the separated control schemes, acting on different time-scales, into one unified grid control scheme.

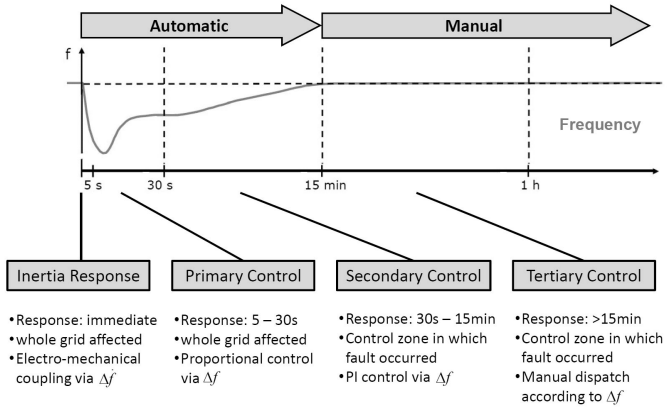

Fig. 1: Classification of conventional grid frequency regulation.

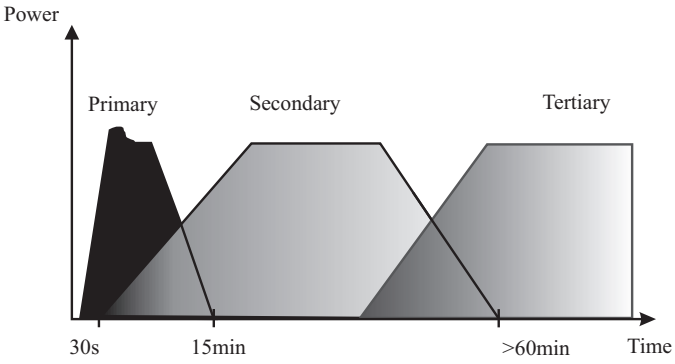

Fig. 2: Conventional grid control reaction after a fault event.

III. The benefits of supplementary control reserve capacity

Several benefits of providing supplementary control reserve capacity can be envisioned. Two of those are discussed here in more detail. First of all, increasing the available quantity of control reserve capacity increases the transmission grid's stability reserve margin in critical situations. This means that the transmission grid's flexibility or robustness when reacting to fault events increases. Combining control reserve capacities from conventional sources as well as from time-variant sources, while explicitly taking into account any constraints that are implied by this time-variability, enables the full utilisation of potentially available control reserve power from all connected sources, i.e. controllable generators and loads. This results in a larger available reserve capacity that can be called upon in an emergency situation.
Second, aggregating control reserve power from time-varying renewable energy sources like onshore and offshore wind

turbines as well as PV arrays, adds the notion of controllability over these energy sources. The formerly uncontrolled fluctuating electric power in-feed from these sources is then at least partially controllable via measures such as partial generation curtailment or delta operation mode [8].

In transmission grids with substantial renewable energy sources (RES) shares, which will most probably be the norm in most OECD countries in a few years due to ambitious renewable energy targets [9]–[11], the fluctuating electricity in-feed should not any longer be understood simply as a disturbance on the grid and as an inherently uncontrollable phenomenon. Controlling the fluctuating RES power in-feed is possible.

Achieving this goal will need updated and possibly new grid management schemes. One of them could be an ancillary service manager that is able to allocate and dispatch supplementary control reserve from time-variant, only partially controllable, sources. Not using the described additional control reserve power to the fullest extent deprives the transmission grid and the existing grid control schemes of potentially available control actuator power as leverage for grid control.

A widely popularised idea for providing additional control reserve capacity is the utilisation of battery storage capacity of PHEVs and the capability to modulate the aggregated load profile from demand side management (DSM) schemes as well as the curtailment of fluctuating electricity in-feed from renewable sources to offer additionally control reserve capacity. This is seen as beneficial especially in regions with a large share of fluctuating electricity in-feed from renewable energy sources [12].

However, the potentially useful control reserve capacity coming from either PHEV batteries, DSM schemes or RES power in-feed has a highly fluctuating availability – depending on week day, time of the day and prevailing electricity consumption patterns. For wind turbines or PV installations the availability depends on wind or solar insolation predictions.

Having reliable predictions on the availability of control reserve power is thus crucial. Furthermore, a management scheme that can explicitly incorporate such predictions and the assumed prediction error would be needed. The concepts for implementing this idea for practical purposes and effectively integrating supplementary control reserve capacity into existing ancillary service frameworks are still in the process of being developed. Though, some promising results exist already [13], [14].

The ultimate usefulness of supplementary control reserve capacity from time-varying sources depends on two questions:

1) Can supplementary control reserve capacity from time-varying sources be integrated in a useful manner in existing ancillary service frameworks?
2) Can the existing ancillary service frameworks be adopted and made more flexible such that the integration of certain sources for supplementary control reserve capacity is facilitated?

Most existing allocation frameworks for ancillary services, i.e. primary and secondary control reserve (= influence on power quality) as well as tertiary control reserve (=influence on power flow), are unfortunately rather rigid [1].

The restrictions are manyfold and range from nominal availability during rather long time-periods, i.e. one week to one month, to the ability to modulate power in-feed to the grid for a given fixed time interval, from quasi-instantaneously after a fault up to hours, see Fig. 2. Additionally, strict constraints on reaction time and power ramp-up and ramp-down rates have to be fulfilled as part of pre-qualification procedures [1], [15].

Within such rigid allocation frameworks, potentially usable control reserve power from time-variant sources cannot be used. The first two criteria regarding fixed availability of control reserve power are the most difficult to fulfill for time-variant generation or storage sources. This is certainly true for wind turbines and PV installations as the accuracy of weather predictions deteriorates dramatically when looking farther out than one or two days ahead [16]–[18]. On the other hand, the latter two criteria regarding reaction time and power ramp rates are often fairly easy to fulfill, certainly when using batteries for providing additional control reserve power.

Making existing ancillary service procurement more flexible would add an important degree of freedom for the integration of time-variant sources [2]. Control reserve capacity for primary and secondary control is usually reserved as fixed capacity for time periods of one week to one month, e.g. *Provide 10 MW (positive and/or negative) secondary control reserve capacity, available at all times, for the whole month of January 2010.* As a simple example, only 38.2% (0.0%) of total battery capacity from an aggregated PHEV fleet of several thousand cars may be available for providing fixed positive (negative) control reserve power at all times during a given time period, here one day (24 h), see Fig. 3. If instead positive (negative) control reserve power could be allocated on an hourly basis, which would be reasonable for the case of a PHEV fleet with a well predictable availability profile, most of the additional control reserve power, 95.3% (76.0%), could be allocated in a reliable manner. In practise, only the above stated sub-optimal, i.e. fixed, allocation of the theoretical available reserve capacity from such sources is possible.

It has to be noted as well that first steps towards making the procurement of ancillary services more flexible have been accomplished recently. Some European TSOs, for example the Swiss TSO swissgrid, have recently changed control reserve capacity auctions for primary and secondary control reserve from monthly to weekly periods, due to the observed lack of liquidity in the capacity auctions [19]. Shorter allocation periods for ancillary services, allow a more flexible procurement of control reserve capacity also from conventional generation. It is conceivable to organise ancillary service auctions on even shorter time horizons, for example on the basis of one- or two-day-ahead auctions, since weather predictions on such short time horizons are relatively accurate [16]. This would enable a more efficient and robust utilisation of control reserve power from wind turbines and PV installations.

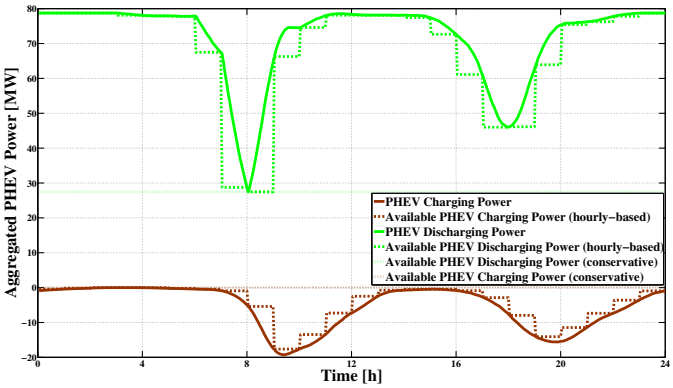

Fig. 3: PHEV Ancillary Service Availability for one day (24 h). (Details are in Section VI.B.)

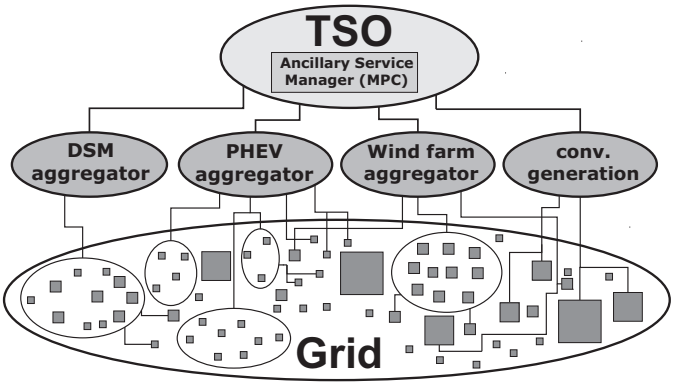

Fig. 4: Communication structure of ancillary service manager to lower level controllers.

IV. Framework of the Ancillary Service Manager

The here proposed ancillary service manager is driven by an MPC setup that allows both the management of control reserve capacity and its utilisation for grid control purposes. It could aggregate control reserve capacity from both fully-dispatchable sources, e.g. conventional generators, as well as from time-variant sources, e.g. PHEV fleets, DSM schemes, curtailable wind generators and PV installations. The manager directly implements general frequency control with the aggregated power reserves while optimally dispatching them from his given portfolio of available capacity according to the grid's needs. Thereby the manager minimises usage costs for the control actuators, respecting technical constraints like ramp rates and time-variant availability of some actuators. In order to efficiently procure grid stability, complete information on the network state is crucial. Typically, TSOs have this information available, hence the manager is resided there.

Both tasks, aggregation and optimal dispatch as well as grid control, are defined, in a first stage, via a conventional MPC setup that can be solved on-line. The actual implementation is then, in a second stage, realised in the form of an explicit MPC scheme that is pre-computed off-line. Therefore, the employed explicit MPC scheme can react in real-time to occurring grid disturbances.

For the effectiveness of this ancillary service manager, both its communication structure with underlying aggregating entities and the employed MPC setup are key factors. The potential communication structure is depicted in Fig. 4. The blocks depicted on the grid level symbolise conventional generators and storages (larger blocks), wind farms (mid-sized blocks) and PHEVs as well as DSM-controlled consumers (small to mid-sized blocks).

The manager communicates either directly with the conventional generation and storage units or indirectly, via aggregator entities with distributed, smaller generation and storage units. The manager continuously sends out control signals and receives information on unit availability and technical constraints, which are used for periodical updates of the MPC setup.

V. MPC Setup of the Ancillary Service Manager

Model predictive control (MPC) is a widely accepted control methodology, combining features of optimal and predictive control. MPC traditionally involves the iterative solution of a constrained finite-time optimal control (CFTOC) problem for the system state $x(k)$ of a given plant model at each sampling step k for a finite prediction horizon $T_p = N * k$, i.e. $[k, k + N * k]$. In each iteration only the first step $u(k)$ of the full cost-minimising control strategy $[u(k), \ldots, u(k + N * k]^T$ is implemented. This optimisation is then repeated, starting with the new system state $x(k + 1)$ [20], [21].

The advantages of MPC are that constraints on the system state x and the control input u can be handled explicitly in the design stage of the CFTOC problem. Furthermore, optimal performance as well as closed-loop stability can be guaranteed through the incorporation of additional constraint equations into the MPC setup [22]–[26].

A. Constrained Finite-Time Optimal Control Problem

A general discrete-time linear time-invariant (LTI) system can be described in state-space form as follows

$$\begin{aligned} x(k+1) &= Ax(k) + Bu(k) \\ y(k) &= Cx(k) + Du(k) \end{aligned} \tag{2}$$

and subjected to general linear inequality constraints

$$\begin{aligned} u \in \mathbb{U} &= g_x^T x(k) \leq 0^T, \ k = 0, ..., N \\ x \in \mathbb{X} &= g_u^T u(k) \leq 0^T, \ k = 0, ..., N-1, \end{aligned} \tag{3}$$

where $x \in \mathbb{R}^n$ is the discrete state vector with $x(0) = [x_1(0), ..., x_n(0)]^T = x_0$, $u \in \mathbb{R}^m$ the discrete control input vector, y the system output, $T_p = N * k$ the prediction horizon, $A \in \mathbb{R}^{n \times n}$ and $B \in \mathbb{R}^{n \times m}$. The $q = q_x + q_u$ constraints imposed on the system state x and

control input u are defined by the vectors $g_x \in \mathbb{R}^{m \times q_x}$ and $g_u \in \mathbb{R}^{m \times q_u}$ respectively.

This system definition for a linear time-invariant (LTI) system can be extended with ease to so-called piece-wise affine (PWA) systems. PWA systems represent the most simple extension of linear systems [27] and allow to model nonlinear and non-smooth processes like a switch between different system dynamics. In the case of the proposed ancillary service manager, this allows to design a sophisticated finite state automaton with different control dynamics for every automaton state. More details on this are given in Section . General PWA systems are defined as follows

$$\begin{array}{rcl} x(k+1) & = & A_i x(k) + B_i u(k) + f_i \\ y(k) & = & C_i x(k) + D_i u(k) + g_i \end{array} \forall \left[\begin{array}{c} x(k) \\ u(k) \end{array} \right] \in \Omega_i, \quad (4)$$

where Ω_i are convex polyhedra defined by a finite number of linear inequalities in the input and state space $\Omega \in \mathbb{R}^{n+m}$ with $\Omega_i \subset \Omega$. The variables $x(k) \in \mathbb{R}^n$, $u(k) \in \mathbb{R}^m$ and $y(k) \in \mathbb{R}^l$ denote the system state, input and output, respectively, at time instant k.

Considering now the task of regulating either an LTI system (Eq. 2) or a PWA system (Eq. 4) with respect to any imposed constraints (Eq. 3) towards the origin, the following cost function needs to be introduced.

$$\begin{aligned} J(u, x_0) &= L_N(x(k+N*k)) + \sum_{k=0}^{N-1} \left(L_k(x(k), u(k))\right) \quad (5) \\ &= \|\mathrm{Q_f} x(k+N*k)\|_l + \sum_{k=0}^{N-1} \left(\|\mathrm{Q}x(k)\|_l + \|\mathrm{R}\delta u(k)\|_l\right), \end{aligned}$$

where $L_k \in \mathbb{R}^{n \times m}$ represents the so-called *stage cost* and $L_N \in \mathbb{R}^{n \times m}$ the so-called *terminal state cost*. The optimisation vector for this minimisation problem is given by $u^* := [u(0)^T, \ldots, u(N-1)^T]^T \in \mathbb{R}^{mN}$, which consists of all decision variables, e.g. control inputs, for $k = 0, ..., N-1$. The cost function is given via the weighting matrices Q, the cost term for system state $x(k)$, $\mathrm{Q_f}$, the cost term for the system state at the end of the prediction horizon $x(k+N*k)$, and R, the cost term for the control input $u(k)$. The term l in $\|\cdot\|_l$ specifies the chosen norm for the cost function as $l \in \{1, 2, \infty\}$.

Obtaining optimal control moves over the given prediction horizon is then equivalent to solving the constrained finite-time optimal control (CFTOC) problem for an LTI or PWA system

$$\begin{aligned} u^* \quad = \quad & \min_{u(\cdot)} \Bigg[\|\mathrm{Q_f} x(k+N*k)\|_l \\ & + \sum_{k=0}^{N-1} \left(\|\mathrm{Q}x(k)\|_l + \|\mathrm{R}\delta u(k)\|_l\right) \Bigg] \quad (6) \end{aligned}$$

$$s.t. \quad \begin{cases} x_0 = x(0) \\ x(k+1) = Ax(k) + Bu(k) \quad \text{(LTI)} \\ \\ x_0 = x(0) \\ x(k+1) = f_{PWA}(x(k), u(k)) \\ \forall \, [x(k), u(k)]^T \in \Omega \quad \text{(PWA)} \end{cases}$$

$$\begin{aligned} & g_x^T x(k) \leq 0^T, \ k = 0, ..., N \\ & g_u^T u(k) \leq 0^T, \ k = 0, ..., N-1 \end{aligned}$$

$$\begin{cases} \mathrm{Q} = \mathrm{Q}` \succeq 0, \mathrm{Q_f} = \mathrm{Q_f}` \succeq 0, \mathrm{R} = \mathrm{R}` \succeq 0, \ \text{if } l = 2 \\ \mathrm{rank}(\mathrm{Q}) = n, \ \mathrm{rank}(\mathrm{R}) = m, \ \text{if } l \in \{1, \infty\}. \end{cases}$$

For the given problem of control reserve capacity aggregation and grid frequency regulation, MPC is a good implementation choice for three reasons:

First, the aggregation of control reserve capacity from time-invariant conventional sources as well as time-variant sources can be implemented in an MPC setup with relative ease via additional constraint definitions for the control actuators $u = [u_1, \ldots, u_m]^T$. In the case of a source for which the availability to provide control reserve power varies over time, time-variable constraints, e.g.

$$u_i^{min}(k) \leq u_i(k) \leq u_i^{max}(k), \quad (7)$$

can be incorporated. In this case, the MPC setup and the MPC control law need to be updated, respectively recomputed, accordingly.

Second, MPC's predictive notion allows an MPC controller to anticipate, via its internal grid model, the abrupt sinusoidal grid frequency swings occurring immediately after a fault event, counter-acting this swing behavior directly instead of merely reacting to it as a P/PI controller would do.

Third, through the MPC setup's cost function of an can explicitly weigh between the gravity of occurring grid frequency deviations Δf in the system state $x = [\Delta f_1, \ldots, \Delta f_n]^T$ and the effort of calling upon reserve capacity ΔP for frequency control via the control inputs $u = [\Delta P_1, \ldots \Delta P_m]^T$. Aggregated control reserve power can optimally be dispatched, i.e. chosen, from the given portfolio of available control reserve capacity according to the grid's needs, while minimising usage costs for the control actuators and respecting technical constraints like ramp rates and time-variant availability of some actuators. In the case of having aggregated battery capacity from PHEV fleets as additional control reserve capacity at disposal, this dynamically fast reacting battery capacity could be used for the control of relatively small and transient frequency disturbances. The use of conventional reserve capacity, say

in the form of a dynamically slow reacting coal-fired power plant, would then only be triggered in case of a large fault in which the control power delivered from the aggregated PHEV fleets is at saturation or in case of a persisting fault with sign bias that would, over time, substantially reduce the PHEV batteries' state-of-charge. Such a behavior can be realised with the help of the above mentioned finite state automaton using PWA sub-systems.

B. Explicit MPC

MPC in its traditional on-line form has a drawback originating from its, in general, time-consuming on-line solution of the CFTOC optimisation problem. The restrictiveness of MPC's computational burden manifests itself in practice through the use of control hardware with limited computational performance, often associated with exponential economical costs.
Thus the applicability of on-line MPC is restricted to processes with relatively slow dynamics. Unfortunately small sampling times are necessary for the control of processes with fast dynamics, as is the case for grid frequency control. This limitation has motivated the search for new solution methods for the optimisation problem that take advantage of pre-computing an optimal control law over all feasible states. Through this process, the computational burden is shifted off-line. Such methods have been presented for linear systems and can be extended to linear hybrid systems in piecewise affine (PWA) form, for both linear and quadratic cost functions [28]–[31].
Techniques exist that allow for both LTI and PWA systems an off-line calculation of an explicit linear MPC control law in the form

$$u_j(x) = K_j\, x + C_j, \quad \text{with } x \in P_j \subset \Omega_i, \tag{8}$$

where $x \in \mathbb{R}^n$ represents the system state and $u_j \in \mathbb{R}^m$ is the valid control input for the region P_j defined within partition Ω_i of the sub space.
The MPC setup parameters that play an important role with respect to the complexity of the explicit MPC controller solution and hence the necessary off-line computational cost, for both LTI and PWA systems, are the employed prediction horizon T_p, which has an exponential influence on the cost [32] and the choice of state and input constraints. The latter are important with respect to feasibility concerns and might lead to numerous extra iterations in the optimisation calculation. For PWA systems, increasing the number of linear subsets linearly increases the computational cost in the off-line stage.

C. Implementation of the Ancillary Service Manager

The actual implementation of the proposed ancillary service manager is realised as follows.
The plant model that is given as an internal model to the MPC-driven ancillary service manager is the classical linearised swing equation in its aggregated form

$$\Delta\dot{f} = \frac{f_0}{2HS_B}(\Delta P_m - \Delta P_{load}) - \frac{f_0}{2HS_B D_{load}}\Delta f - \frac{W_0}{HS_B}\Delta\dot{f}, \tag{9}$$

where f is the centre of inertia grid frequency, H the total inertia constant of all generators of a given grid model, S_B the total rating of the generators, P_m the total mechanical power of the generators and P_{load} the total system load of the grid. The constants D_{load} and W_0 describe the frequency dependency of the system load. Equation 9 is valid for the case of an assumed highly meshed grid system, in which all units can be assumed to be connected to the same grid bus, representing the centre of inertia of the given grid [33]. Further details are given in Section VII.

Using $x_f := \Delta f, x_f(0) := f_0$ and $u := (\Delta P_m - \Delta P_{load})$, Eq. (9) can be rephrased as

$$\dot{x}_f = \frac{x_f(0)}{2HS_B}u - \frac{x_f(0)}{2HS_B D_{load}}x_f - \frac{W_0}{HS_B}\dot{x}_f. \tag{10}$$

In this study only PHEVs are considered for providing supplementary control reserve power. Several PHEV fleets with differing drive profiles as well as differing aggregated state-of-charge (SOC) are considered for this task. In order to ensure that a PHEV fleet's aggregated SOC is not depleted over time, an additional system state x_{SOC_i} is created for every PHEV fleet i and incorporated into the manager's MPC setup. The corresponding state-space equation as

$$x_{SOC_i}(k+1) = x_{SOC_i}(k) - K_i\, u_{PHEV_i}(k), \tag{11}$$

where x_{SOC_i} is the aggregated state-of-charge (SOC) of a given PHEV fleet i and u_{PHEV_i} is the control actuator input that supplies control reserve power to the grid. K_i is the constant factor that links control actuator usage and SOC depletion.
The approach allows to specify constraints for every state $x_{SOC_i}(k)$, bounding it to a pre-defined operating range, i.e. $x^{min}_{SOC_i} \leq x_{SOC_i(k)} \leq x^{max}_{SOC_i} = 1.0$. Furthermore, deviations from a PHEV fleet's nominal $x^0_{SOC_i}(k)$ can be penalised in the MPC cost function via the matrices Q and $\mathrm{Q_f}$, which leads to a replenishment of the state-of-charge during time periods without fault events.
Taking advantage of the degree of freedom that the design of PWA systems offers, a finite state PWA automaton can be modelled that incorporates different linear sub-systems, which either allow or prohibit the usage of certain control reserve actuators u_i. Some of the system states x_i can then be used to trigger a switch from one system dynamic to another. As an example, the continued use of control reserve power from PHEV fleet i over time degrades this fleets SOC, x_{SOC_i}. Eventually reaching a pre-defined lower limit for x_{SOC_i} triggers a switch in system dynamics from the present PWA sub-system *PWA*$_j$, which only foresaw the usage of control reserve power from r PHEV fleets $[u_{PHEV_1}, \ldots, u_{PHEV_r}]$, to another PWA sub-system *PWA*$_k$, which also allows the usage of control reserve power from a conventional generator $[u_{conv_1}, \ldots, u_{conv_s}]$. The MPC controller would then alleviate the burden from the

excessively used PHEV control actuators and gradually replace it with the control actuators of the conventional generators. The same switch in system dynamics would be initiated in case of a single persisting fault with sign bias that would, over time, also substantially reduce the PHEV batteries' state-of-charge. An additional system state x_{fault} can be introduced that triggers a switch in system dynamics as soon as a pre-defined threshold value C_{fault} for PHEV control actuator usage is reached, e.g.

$$\dot{x}_{fault} = \sum_{i=1}^{i=r} u_{PHEV_i}(k) \tag{12}$$
$$\text{with} \begin{cases} \text{if } |x_{fault}| \geq |C_{fault}|, \ PWA_j \rightarrow PWA_k \\ \text{if } |x_{fault}| < |C_{fault}|, \ PWA_k \rightarrow PWA_j \end{cases}$$

A similar trigger can be designed for the case, where the required control actuator response $u_{required}$ to a large fault immediately saturates the control actuators of all participating PHEV fleets $u_{PHEV_1}, \ldots, u_{PHEV_r}$, i.e. $\sum_{i=1}^{i=r} u_{PHEV_i}^{max}(k) < u_{required}(k)$ or $\sum_{i=1}^{i=r} u_{PHEV_i}^{min}(k) > u_{required}(k)$. (The following holds: $u_{PHEV_i}^{max} \geq 0$, $u_{PHEV_i}^{min} \leq 0, \forall i$. A switch to a PWA sub-system PWA_k that allows the additional usage of control actuators from conventional generators, $u_{conv_1}, \ldots, u_{conv_s}$ would then take place. Within PWA_k the following holds: $\left(\sum_{i=1}^{i=r} u_{PHEV_i}^{max}(k) + \sum_{i=1}^{i=s} u_{conv_i}^{max}\right) < u_{required}(k)$. An illustration of the finite state PWA automaton and the switching procedure is shown in Fig. 5.

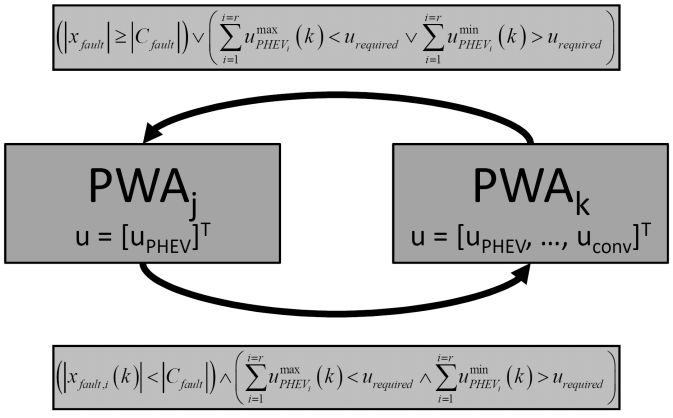

Fig. 5: a) PWA Automata (PHEV and conventional reserve capacity). Switching behaviour for the case of control input saturation and SOC depletion.

Due to the incorporation of the above discussed additional system states, the resulting full system state vector x and the full control actuator vector u of the ancillary service manager are thus given as

$$x(k) = [x_f(k), x_{SOC_1}(k), \ldots, x_{SOC_r}(k), x_{fault}(k)]^T \tag{13}$$

$$u(k) = [u_{PHEV_1}(k), \ldots, u_{PHEV_r}(k), u_{conv_1}(k), \ldots, u_{conv_s}(k)].^T \tag{14}$$

All constraints, both time-invariant and time-variant, for system states as well as for control actuators can be posed in the following uniform way

System state (15)

$$-0.5\,Hz = x_f^{min} \leq x_f \leq x_f^{max} = +0.5\,Hz \tag{15a}$$
$$0.20\,pu = x_{SOC_i}^{min} \leq x_{SOC_i} \leq x_{SOC_i}^{max}(k) \leq 1.0\,pu \tag{15b}$$

$\forall i = 1, \ldots, r$

Conventional control reserve capacity

$$u_{conv_i}^{min.} \leq u_{conv_i} \leq u_{conv_i}^{max.} \tag{15c}$$
$$\dot{u}_{conv_i}^{min.} \leq \dot{u}_{conv_i} \leq \dot{u}_{conv_i}^{max.} \tag{15d}$$

$\forall i = 1, \ldots, s$

Supplementary control reserve capacity

$$u_{PHEV_i}^{min.}(k) \leq u_{PHEV_i} \leq u_{PHEV_i}^{max.}(k) \tag{15e}$$
$$\dot{u}_{PHEV_i}^{min.}(k) \leq \dot{u}_{PHEV_i} \leq \dot{u}_{PHEV_i}^{max.}(k) \tag{15f}$$

$\forall i = 1, \ldots, s,$

where equation (15a) sets a safety limit for the maximal allowable frequency deviation $x_f := \Delta f$ and (15b) sets the permissible operation range for the aggregated state-of-charge x_{SOC_i} of the r available PHEV fleets. All control actuator constraints of the s conventional units are set to be time-invariant: equation (15c) sets the permissible operation range of the power rating, while (15d) is defining the permissible power ramp rates. All control actuator constraints of the r PHEV fleets are defined as being time-variant: equation (15e) sets the permissible operation range of the power rating, while (15f) is defining the permissible power ramp rates.

VI. Simulation and aggregation of individual PHEVs for control purposes

The individual behavior of PHEVs is fundamental for the provision of control reserves. In order to create a realistic situation in which the PHEVs incorporate a temporal variability in their connection pattern and their SOC, the vehicles have been simulated individually. Section VI-A introduces the single PHEV model in order to illustrate how information on the SOC of an individual PHEV is attained. Subsequently, section VI-B introduces the aggregation procedure which determines the necessary control states and inputs to the MPC framework, i. e. the SOC and the available regulation power. Both are based on the results of the single PHEV model.

A. The single PHEV model

Clearly, a PHEV's main function is for transport. However, unlike combustion engine vehicles they can also be utilised for ancillary services in power systems. In order to model the potential utilization of the vehicles for such modes, several

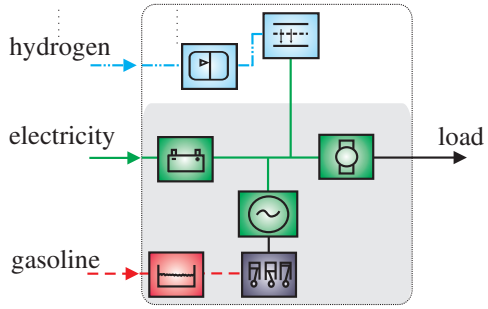

Fig. 6: PHEV with fuel cell modelled as an energy hub

PHEV operating states have been defined in [5]. They comprise the driving state (D), the charging state(C), the refuelling state (RF) and possibly offering ancillary services (R) and are denoted in Eq. (16). The charging state can be integrated into the ancillary services state. A situation decision function given in (17) is defined in order to integrate the different states into a PHEV model.

$$\Xi = \{\mathtt{D}, \mathtt{C}, \mathtt{RF}, \mathtt{R}\} \tag{16}$$

$$\mathcal{E}(\Xi) = \frac{\partial}{\partial \Xi} \begin{pmatrix} \mathtt{D} & \mathtt{C} & \mathtt{RF} & \mathtt{R} \end{pmatrix} \tag{17}$$

Recently, the energy hub approach [34] has been used to model PHEVs [5]. This PHEV model, illustrated in Fig. 6, is used here to determine the battery state of PHEVs incorporating different daily temporal behaviors. The vehicle model is given in Eq. (18), where **L** denotes the load of the PHEV hub, **C** is the coupling matrix between the used energy carriers, here electricity and gasoline, **S** is the storage matrix, **P** is the input to the hub and $\dot{\mathbf{E}}$ is the storage input.

$$\mathbf{L} = \mathcal{E}(\Xi) \begin{pmatrix} \mathbf{C} & -\mathbf{S} \end{pmatrix} \begin{pmatrix} \mathbf{P} \\ \dot{\mathbf{E}} \end{pmatrix} \tag{18}$$

with

$$\mathbf{C} = \begin{pmatrix} c_{el\,kin\,\mathtt{D}}(\mathbf{L}) & c_{gaso\,kin\,\mathtt{D}}(\mathbf{L}) & 1 \\ 1 & 0 & 0 \\ 0 & 1 & 0 \end{pmatrix} \tag{18a}$$

$$\mathbf{S} = \begin{pmatrix} \frac{c_{el\,kin\,\mathtt{D}}(\mathbf{L})}{\eta_{el}} & \frac{c_{gaso\,kin\,\mathtt{D}}(\mathbf{L})}{\eta_{gaso}} \\ \frac{1}{\eta_{el}} & 0 \\ 0 & \frac{1}{\eta_{gaso}} \end{pmatrix} \tag{18b}$$

and

$$\mathbf{P} = \begin{pmatrix} P_{el\,\Xi} \\ P_{gaso\,\Xi} \\ P_{dis} \end{pmatrix} \quad \dot{\mathbf{E}} = \begin{pmatrix} \dot{E}_{el} \\ \dot{E}_{gaso} \end{pmatrix} \tag{18c}$$

The load of the PHEV when driving is calculated through Newton's Second law given in (19). Here M is the vehicle's mass, v is the speed, C_r is the tire friction coefficient, A_f is the cars front area, C_D is the car air resistance coefficient, ρ_{air} is the air density, δ is the vehicle mass coefficient and $\sin(\Theta)$ is the road's grade.

$$E = (MgvC_r + \frac{1}{2}\rho_{air}C_D A_f v^3 + \delta M v\dot{v} + Mgv\sin(\Theta))\Delta \tag{19}$$

Utilising linear optimization, the hub formulation can be used to simulate PHEVs in charge depleting and, if the SOC is low, in charge sustaining mode. The optimization problem is given in (20) is minimizing total fuel costs for transport. The hub formulation assures that the kinetic load is supplied either by the battery or by the gasoline tank. The first two constraints refer to minimum and maximum power output of the ICE and the battery, respectively. Constraint (20c) gives that the SOC of the battery needs to lie between 100% and 20%. Constraints (20d) and (20e) refer to the power derivative bounds of the engine (ICE) and the electric motor. For the ICE usage a heuristic was chosen and implemented through the constraints (20f) and (20g). The heuristic bounds the converter to a minimum of 300 seconds of running time once it is switched on. Also, the minimum power output of the last optimization step is taken as the lower bound for the ICE operation in the next step through (20h). The last constraint refers to the dissipated power in each step. A complete overview of the vehicle parameters, which are used to model the PHEV energy hub, is found in [5].

$$min \quad \mathscr{F}^T(\dot{E}_{el}^T, \dot{E}_{gaso}^T) \tag{20}$$

$$s.t. \quad \mathbf{L} = \mathcal{E}(\Xi) \begin{pmatrix} \mathbf{C} & -\mathbf{S} \end{pmatrix} \begin{pmatrix} \mathbf{P} \\ \dot{\mathbf{E}} \end{pmatrix} \tag{20a}$$

$$\delta_{gaso}\underline{\dot{E}}_{gaso\,\mathtt{D}}^T \leq \dot{E}_{gaso\,\mathtt{D}}^T \leq \overline{\dot{E}}_{gaso\,\mathtt{D}} \tag{20b}$$

$$\underline{\dot{E}}_{el\,\mathtt{D}} \leq \dot{E}_{el\,\mathtt{D}}^T \leq \overline{\dot{E}}_{el\,\mathtt{D}} \tag{20c}$$

$$\underline{SOC} \leq SOC^T \leq \overline{SOC} \tag{20d}$$

$$\underline{\dot{P}}_{el\,\mathtt{D}} \leq \frac{d\dot{E}_{el\,\mathtt{D}}^T}{dt} \leq \overline{\dot{P}}_{el\,\mathtt{D}} \tag{20e}$$

$$\underline{\dot{P}}_{gaso\,\mathtt{D}} \leq \frac{d\dot{E}_{gaso\,\mathtt{D}}^T}{dt} \leq \overline{\dot{P}}_{gaso\,\mathtt{D}} \tag{20f}$$

$$\delta_{gaso} = 1 \; if \dot{E}_{gaso\,\mathtt{D}}^T \geq 0 \wedge t_{gaso} \leq 300 \tag{20g}$$

$$\underline{\dot{E}}_{gaso\,\mathtt{D}}^{T+1} = \dot{E}_{gaso\,\mathtt{D}}^T \tag{20h}$$

$$P_{dis} \leq 0 \tag{20i}$$

The output of the PHEV mode is illustrated in Fig. 7, where (a) shows different drive cycles and their speed profile, which a PHEV can be envisioned to have in the real world. Figure 7(b) gives the power demanded by the drive cycles. Figure 7(c) shows the power drawn from the battery and (d) the resulting SOC. Figure 7 (e) and (f) visualise the ICE utilization.

B. The aggregation of PHEVs for ancillary services

The output of the single PHEV model can be used to simulate large PHEV fleets where the individual cars have different temporal behaviors. Knowing the SOC at the different locations and the vehicle's connection times, the information can be used to aggregate PHEVs into one virtual storage unit.
The single vehicle model was utilized to simulate 84 different drive cycles for 15'000 PHEVs with a specific time distribution. The 84 drive cycles are uniformly distributed between the PHEVs. The cycles are composed from the Urban Dynamic

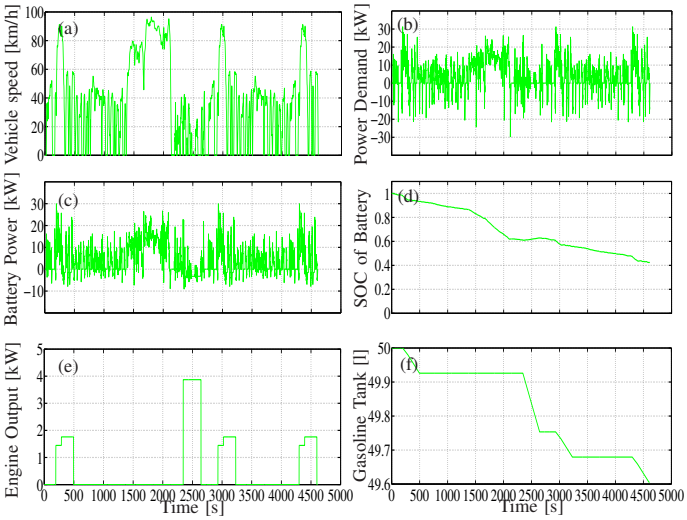

Fig. 7: Simulation of various test driving cycles; see text

(a) Vehicle Speed (b) Demanded Power
(c) Demanded Power from Battery (d) SOC of Battery
(e) Demanded Power from ICE (f) Gasoline Consumption

Fleet #1	12kWh, 3.5kW	**Fleet #2 & #3**	12 & 30kWh, 3.5kW
Dep. Time	15'000 PHEVs	**Dep. Time**	15'000 PHEVs
5-6 am	7.4%	3-6 am	3%
6-7 am	32%	6-7 am	17%
7-8 am	42%	7-8 am	70%
8-9 am	18.6%	8-10 am	10%
Park Time		**Park Time**	
7-8 h	7.4%	7-8 h	3%
8-8.5 h	32%	8-8.5 h	17%
8.5-9 h	42%	8.5-9 h	70%
9-10 h	18.6%	9-10 h	10%

TABLE I: Distribution of departure times of the simulated PHEV fleets

Drive Cycle (UDDS) with 7.9 miles sampled, Highway Fuel Economy Cycle (HWFET) with 10.26 miles sampled, New York City Cycle (NYCC) with 1.18 miles sampled and Federal Test Procedure (FTP) 75 [35]. Here, for simplicity, it is assumed that the PHEVs only travel from home to work and back while pervasive connection points are available.

As soon as the PHEVs connect to the power grid, it is assumed that they are managed by a PHEV aggregator [3]. This aggregator, taking advantage of advanced metering interfaces, is situated between the distribution system operator (DSO), the PHEVs and the TSO. The aggregator signs the PHEVs into its V2G management framework as soon as they connect to the network. Although, various PHEV management schemes like controlled recharging (i.e. load management [36], [37]) or even uncontrolled recharging can be envisioned, the PHEVs are considered here only for V2G services [6]. Quitting V2G services and transferring into other possible modes in order to sufficiently be recharged for the next trip is neglected. The simplification can easily be introduced for PHEVs due to their ICE acting as an ancillary power source for propulsion.

The aggregator assesses the maximal power available for up and down regulation in each time step. In case the PHEV k is recharging with a power $\mathfrak{p}_k^c(t)$, its SOC is updated for the next interval. The assessment of the storage capacity is denoted in Eq. (21), where $P_{pos}^{reg}(t), P_{neg}^{reg}(t)$ give the positive and negative control power reserves in time step t. Further, $C_k^p, C_k^B, SOC_k(t), \eta$ denote the power connection capacity, the battery capacity, the actual state of charge and the charging efficiency for the k-th car from the set of connected PHEVs denoted $\mathcal{PHEV}(t)$, respectively.

$$\begin{aligned} &\textit{Positive Control} \begin{cases} P_{pos}^{reg}(t) = \sum_k (\mathfrak{p}_k^c(t) + C_k^p) \\ SOC_k(t+\delta t) = SOC_k(t) - \frac{C_k^p \delta t}{\eta C_k^B} \end{cases} \\ &\textit{Negative Control} \begin{cases} P_{neg}^{reg}(t) = \sum_k (C_k^p - \mathfrak{p}_k^c(t)) \\ SOC_k(t+\delta t) = SOC_k(t) + \frac{((C_k^p - \mathfrak{p}_k^c(t))\eta)\delta t}{C_k^B} \end{cases} \\ &\forall\, k \in \mathcal{PHEV}(t) = \{1 \dots N_{PHEV_n}\} \end{aligned} \tag{21}$$

The SOC of the aggregated PHEV storage which is denoted SOC_{aggr}^{V2G} can be represented by (22), where $\mathfrak{e}_k$ is the actual energy content of the kth PHEV and C_k^B is its battery size. Using this simple aggregation method, time-variant availabilities of positive and negative control power for different fleet behavior can be calculated. Figure 8 illustrates the three cases which where defined in Table I.

$$SOC_{\text{aggr}}^{\text{V2G}} = \frac{\sum_{k=1}^{N_{PHEV_n}} \mathfrak{e}_k}{\sum_{k=1}^{N_{PHEV_n}} C_k^B} \tag{22}$$

Figure 8(a) illustrates the number of PHEVs connected to the power grid throughout the day. The lines visualize the different behavior of the cars based on the distribution of departure and parking times given in Table I.

Figure 8(b) shows the SOC of the aggregated PHEV storage throughout the day. Here, six different cases are given, as each fleet was either assumed to be recharged with 1.75 kW while connected in V2G mode or not being recharged at all. The first case gives the aggregator the possibility to increase load if it is demanded by the system. This would not be possible if the cars would recharge with their full plug capacity. It can be seen, that the SOC for the recharging cases is much higher throughout the day. For the cases where the PHEVs are not recharged at all, the aggregated SOC is low and decreases to values almost as low as 20% later through the day. This is obviously due to the driving behavior of the fleet. The SOC at the end of the simulation does not equal the one at the beginning, which also relates to the fact of not being recharged. Note that the aggregated SOC for the 30kWh fleet is much larger, even in the evening hours.

Figure 8(c) and (d) show the available power for charging and discharging, respectively. In the cases where the PHEVs are recharged, there are times during which the available power for additional charging becomes zero because the batteries are full. Vice versa, in the case of not recharging the PHEVs at all, the power for discharging becomes very low.

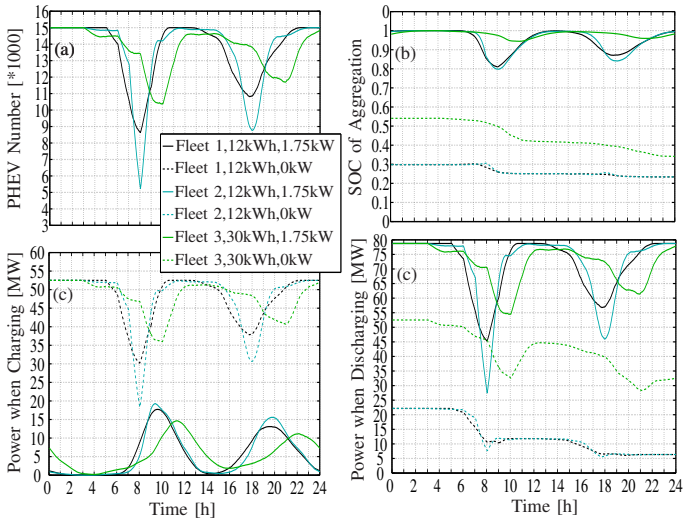

Fig. 8: Simulation of PHEV fleets and their aggregation. The bold lines show the results for fleets charging at 1.75kW. The dashed lines show the results for fleets which are not charging at all throughout the day.

(a) Vehicle number (b) Aggregated SOC of storage
(c) Power when charging (d) Power when discharging

VII. Benchmark transmission grid

The control performance of the ancillary service manager is tested on a IEEE 14 bus system. It consists of five generation nodes, nine load nodes and interconnecting power lines. Simulation results presented here are based on the dynamical data and grid topology for the system, as presented in [33], [38], seen also in Table II.

The use of the IEEE 14 bus benchmark system is a reasonable choice, since its rather small size provides a good trade-off between being a grid model with representative dynamics and offering a reasonable computational effort for simulations.

Figure 9 is a single line diagram of the benchmark system. Conventional generators are connected to buses 1, 2, 3, 6 and 8. All other buses are load buses. Generator faults are all initiated with the generator at bus 1. The generator at bus 6 can be used by the ancillary service manager for providing conventional control reserve power. The ancillary service manager can additionally use supplementary control reserve power from two PHEV fleets that are connected to load buses 5 and 9, respectively.

The generator dynamics of the benchmark system can be represented by the classical swing equation, e.g.

$$\Delta \dot{f}_i = \frac{f_0^2}{2H_i S_{Bi} f_i} \left(P_{mi} - P_{ei}\right) \;\; \forall\, i = 1, \ldots, n, \qquad (23)$$

where f_i is the frequency at generator bus i, H_i is the inertia constant, S_{Bi} is the rated power, P_{mi} is the mechanical power and P_{ei} is the electrical power of the generator and $f_0 = 50\,Hz$.

Since load-frequency disturbances are normally relatively small, linearised swing equations with $\Delta f_i = f_i - f_0$ can be used [39]. Moreover, an aggregated swing equation for the $n = 5$ generators of the given benchmark grid can be introduced:

$$\Delta \dot{f} = \frac{f_0}{2HS_B}(\Delta P_m - \Delta P_{load}) - \frac{f_0}{2HS_B D_{load}} \Delta f - \frac{W_0}{HS_B} \Delta \dot{f} \qquad (24)$$

with

$$\begin{aligned} f &= \frac{\sum_i H_i f_i}{\sum_i H_i} \\ S_B &= \sum_i S_{Bi} \\ H &= \frac{\sum_i H_i S_{Bi}}{\sum_i S_{Bi}} \\ \Delta P_m &= \sum_i \Delta P_{mi} \\ \Delta P_{load} &= \Delta P_e = \sum_i \Delta P_{ei}, \end{aligned}$$

where f is the centre of inertia grid frequency, H is the total inertia constant of all generators of a given grid model, S_B is the total rating of all generators, P_m is the total mechanical power of all generators and P_{load} is the total system load of the grid. The constants D_{load} and W_0 describe the frequency dependency of the system load. Equation 24 is valid for the case of an assumed highly meshed grid system, in which all units can be assumed to be connected to the same grid bus, representing the centre of inertia of the given grid [33].

The dynamical behavior of the generators in the IEEE 14 bus system for the case of a step-change of generator 1 is depicted in Fig. 10. It can clearly be seen that some of the generators, depending on their individual generator inertia and their respective position within the grid topology, start to swing against each other. This specific dynamic behavior cannot be detected in the aggregated swing equation, Eq. (24), the internal model of the MPC. This clearly constitutes a model-plant mismatch that the MPC controller has to cope with online.

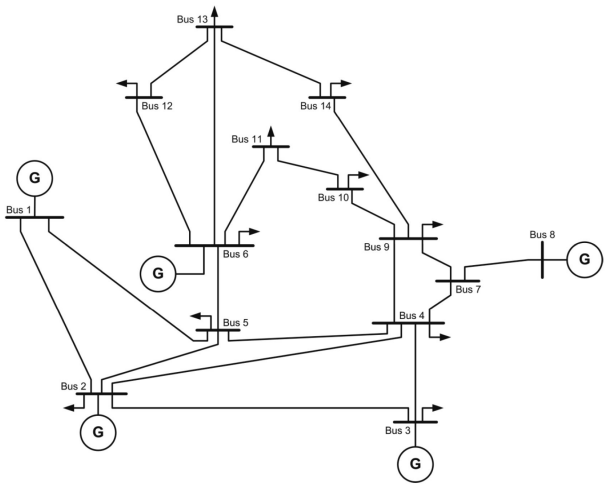

Fig. 9: Topology of the IEEE 14 Bus System.

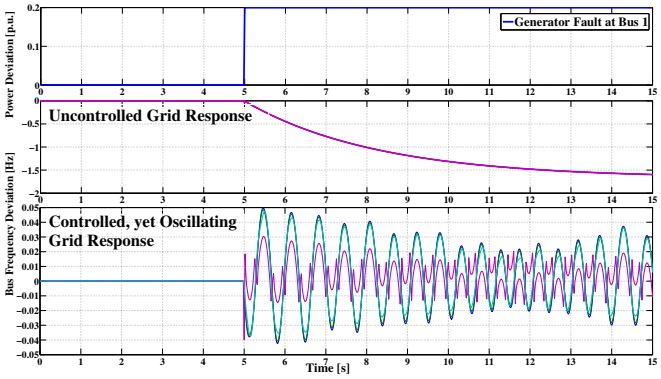

Fig. 10: Dynamical behavior of the IEEE 14 Bus System.

Description	Parameter	Value
Generator Inertia [s]	H_1	8.0
	H_2	8.0
	H_3	8.0
	H_6	8.0
	H_8	8.0
Generator Rating [pu]	S_{B_1}	$0.4951 + j0$
	S_{B_2}	$0.2 + \imath 0$
	S_{B_3}	$0.4 + \imath 0$
	S_{B_6}	$0.5 + \imath 0$
	S_{B_8}	$0.2 + \imath 0$
Loads at Buses [pu]	P_{Load_4}	$-0.4 - \imath 0.5$
	P_{Load_5}	$-0.07 - \imath 0.01$
	P_{Load_7}	$0.0 + \imath 0.0$
	P_{Load_9}	$-0.35 - \imath 0.05$
	$P_{Load_{10}}$	$-0.20 - \imath 0.06$
	$P_{Load_{11}}$	$-0.20 - \imath 0.08$
	$P_{Load_{12}}$	$-0.16 - \imath 0.05$
	$P_{Load_{13}}$	$-0.28 - \imath 0.05$
	$P_{Load_{14}}$	$-0.08 + \imath 0.05$
Load Damping ($\sim f$) [$\frac{Hz}{pu}$]	D_{load}	$\frac{1}{2}$
Load Damping ($\sim \dot{f}$) [$\frac{pu}{Hz}$]	W_0	0

TABLE II: Parameters of the IEEE 14 Bus System ($1.0\,\text{pu} = 100\,\text{MVA}$).

VIII. Simulations

The presented MPC scheme for the ancillary service manager is implemented using the freely available *Multi-Parametric Toolbox* (MPT) [40].

All simulations are run as fixed-step simulations with a sampling time of $T_s = 20\,ms$, using either a first-order ODE solver (Euler method) for longer-term simulations in Matlab or a forth-order ODE solver (Runge-Kutta) for shorter-term simulations in Simulink.

The ancillary service manager is implemented as a fast-responding explicit MPC controller, which can react in real-time to frequency deviations. Any communication and measurement time-delays in the feedback control loop are, for now, neglected. In the longer-term simulations, the time-varying constraints of the different control reserve capacities, notedly of the PHEV fleets' control actuators are updated constantly in intervals of 3 minutes.

The here employed system state vector x and control actuator vector u of the ancillary service manager are given as

$$x = [x_f, x_{SOC_1}, x_{SOC_2}, x_{fault_1}, x_{fault_2}]^T \quad (25)$$

$$u = [u_{PHEV_1}, u_{PHEV_2}, u_{conv}].^T \quad (26)$$

The switching behavior of the PWA automaton is triggered at a value of $|C_{fault}| = 15000$. This corresponds to a fault of $\pm 0.5\ pu$ that endures longer than 10 minutes.

The employed MPC setup is defined as presented in Eq. (6). A finite prediction horizon of $T_p = 3 * k$ was chosen. The weighing matrices of the cost function, Eq. (5) are given as

$$\mathrm{Q} = \begin{bmatrix} 1000 & 0 & 0 & 0 & 0 \\ 0 & 1 & 0 & 0 & 0 \\ 0 & 0 & 1 & 0 & 0 \\ 0 & 0 & 0 & 1 & 0 \\ 0 & 0 & 0 & 0 & 1 \end{bmatrix}, \ \mathrm{R} = \begin{bmatrix} 10 & 0 & 0 \\ 0 & 10 & 0 \\ 0 & 0 & 10 \end{bmatrix}, \quad (27)$$

where Q is the weighing matrix for the system state and R the weighing matrix for the change of the control input $\Delta\left(u(k+1) - u(k)\right)$. The weighing matrix $\mathrm{Q_f}$ for the final system state of the prediction $x(k + N * k)$ is neglected and, hence, set to $\mathrm{Q_f} = 0 * \mathrm{Q}$.

The constraints on the system state and on the control actuators are in line with Eq. (15), but defined here in more detail as

System state (28)

$$\begin{array}{lcccl} -0.5\,Hz = x_f^{min} & \leq & x_f & \leq & x_f^{max} = +0.5\,Hz \\ 0.20\,pu = x_{SOC_i}^{min} & \leq & x_{SOC_i} & \leq & x_{SOC_i}^{max}(k) \leq 1.0\,pu \\ \forall i = 1, \ldots, 2 & & & & \end{array}$$

Conventional control reserve capacity

$$\begin{array}{lcccl} -0.4\,pu & \leq & u_{conv} & \leq & = +0.4\,pu \\ -0.0006666\,pu/s & \leq & \dot{u}_{conv} & \leq & = +0.0006666\,pu/s \end{array}$$

Supplementary control reserve capacity

$$\begin{array}{lcccl} u_{PHEV_i}^{min.}(k) & \leq & u_{PHEV_i} & \leq & u_{PHEV_i}^{max.}(k) \\ \dot{u}_{PHEV_i}^{min.}(k) & \leq & \dot{u}_{PHEV_i} & \leq & \dot{u}_{PHEV_i}^{max.}(k) \\ \forall i = 1, \ldots, 2, & & & & \end{array}$$

where the time-varying constraints of the two PHEV units are derived from the aggregation patterns for a whole day of a PHEV fleet with 2.12 kW charging power, Fig. 8. PHEV fleet 1 is assumed to charge with 1.75 kW and PHEV fleet 2 is assumed to be not charging throughout the day. Furthermore, it is assumed that the PHEV fleets can fully ramp-up/ramp-down their available power rating within 2 seconds. The conventional generator, considered to be a gas turbine, can fully ramp-up/ramp-down the allocated control reserve power at his nominal working point within 30 seconds.

The presented benchmark grid is put under stress by several generator faults, which all occur on bus 1. These faults happen on different time-scales.

First, the stabilising control performance of the explicit MPC controller is tested for short-term generator faults, namely step-change power deviations of -0.2 pu and -0.2 pu, each for 30 s. As can be seen in Fig. 11, all occurring frequency deviations

are rapidly brought back to zero. Noteworthy is that the largest initial frequency deviation, $100\,mHz$, occurs when there is a positive power deviation at $t = 70\,s$. This is explained by the fact that PHEV fleet 1 is already charging at nominal levels and cannot charge electricity at a much higher level. In this situation PHEV fleet 2 is contributing most to the balancing effort. Control reserve power of the conventional unit is not called upon at all, as no PWA switching is triggered for the tested short-term faults.

Second, the stabilising control performance of the explicit MPC controller is tested for longer-term generator faults, namely step-change power deviations of -0.2 pu and -0.2 pu, each for 20 minutes. As is shown in Fig. 12, all occurring frequency deviations are again rapidly brought back to zero. As the persistence of the power deviation eventually triggers a PWA switching, at around $t = 500\,s$, the conventional unit starts to deliver control reserve power and assists the PHEV fleets. After $t = 3600\,s$, when all faults are cleared, the conventional unit recharges both PHEV fleets to nominal state-of-charge levels (till $t = 4800\,s$).

Third, the effective management of the time-varying control reserve capacity from the two PHEV units is put to test. In Fig. 13, it is shown how the control response of the MPC scheme has to change over time, depending on the varying availability of PHEV control reserve power. A given fault event, -0.5 pu occurring at around 7 am ($t = 7\,h * 60\,min. * 60\,s = 25200\,s$) , can be rejected solely by using the available control reserve power of the PHEV fleets. When the same fault occurs an hour later, around 8 am ($t = 8\,h * 60\,min. * 60\,s = 28800\,s$), most of the PHEVs have left for work. Therefore, additional control reserve power needs to be called from the conventional generation unit.

Forth, the MPC schemes control response is tested for severe generator faults that saturate the combined reserve capacity power of the two PHEV fleets. In Fig. 14, it is shown that smaller fault events, -0.5 pu, can effectively be rejected by the two PHEV fleets themselves. However, for the rejection of highly severe faults, here -1.2 pu, the conventional unit is triggered and provides the additionally needed control reserve power.

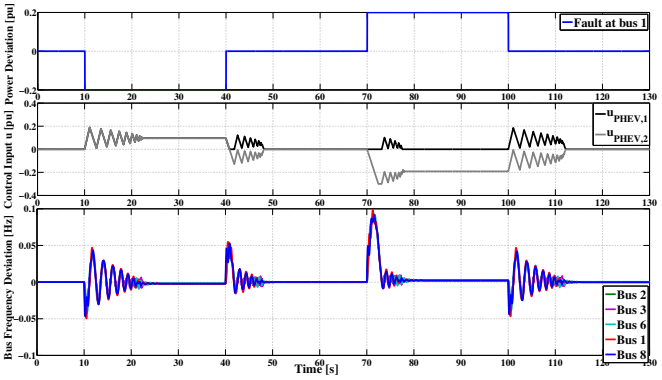

Fig. 11: Stabilising control for short-term faults.

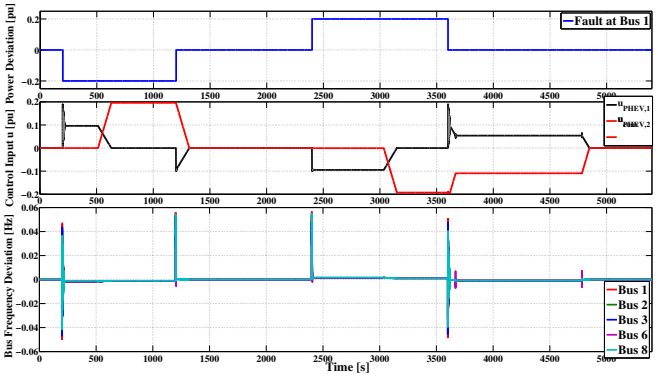

Fig. 12: Stabilising control for long-term faults.

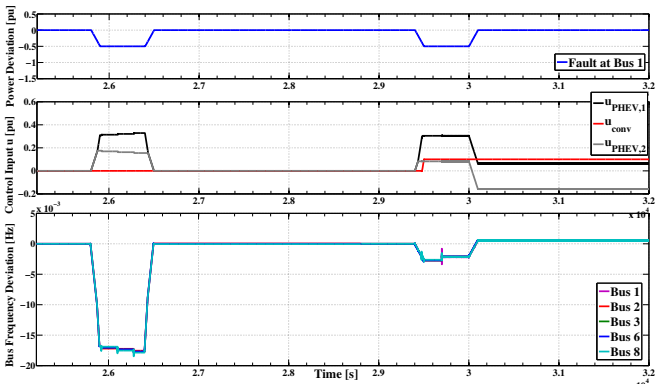

Fig. 13: Stabilising control for time-varying PHEV control reserve power $u_{PHEV_i}(k)$.

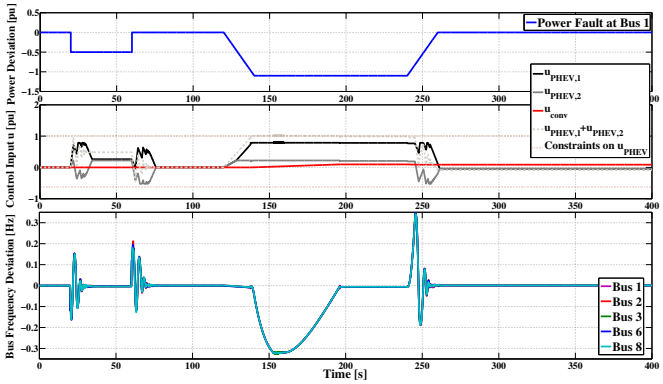

Fig. 14: Stabilising control if PHEV control actuators u_{PHEV_i} are at saturation.

IX. Conclusions

The here proposed methodology for an ancillary service manager proofs to be a viable method for allocating and managing supplementary control reserve capacity from time-variant sources, in this study coming from PHEV fleets. Control reserve capacity from other time-variant sources, such as wind turbines, PV installations and DSM schemes can be implemented with the same allocation method, assuming that appropriate aggregator entities, e.g. an appliance manager [41] or a wind turbine controller [8], exist. All these time-variant sources together constitute a huge albeit still untapped

potential for additional control reserve capacity.

Moreover, the employed MPC scheme shows several advantages for the task of grid frequency control. This is first of all the ability to explicitly incorporate constraints into the control setup. These constraints can be on the state, e.g. the maximal admissible grid frequency deviation in a fault occurrence and the admissible operating range of PHEV batteries' state-of-charge, as well as on the control input, e.g. the admissible operating range of electric power output and the associated ramp rates, into the control setup. Second, the ability for an active coordination of several control actuators within one control scheme. This allows to choose the appropriate control actuator from a portfolio of various control power sources, which have different operating costs and technical constraints, according to the occurred fault event, e.g. short-term fault versus long-term fault. Third, since MPC inherits the properties of optimal control theory, such schemes have fundamental control performance advantages over traditional P/PI schemes, e.g. the optimality of the applied control moves. The design freedom for an MPC setup gained from the usage of piece-wise affine (PWA) systems, implemented as a finite-state automaton, allows to realise switching between different dynamic behaviors of an MPC controller. Thus making it possible to combine conventional primary and secondary control into one unified scheme. Pre-calculating the control strategy of the ancillary service manager as an explicit MPC controller allows to shift the burden-some on-line computational effort of conventional MPC schemes into an off-line stage. This feature allows an explicit MPC controller to react as fast as conventional P/PI/PID controller, i.e. in real-time.

Prior studies have shown that centralised or decentralised MPC schemes can be used effectively for load frequency control, notably for automatic generation control (AGC) [42], [43]. The novel aspect treated here is the idea to realise grid frequency control on different time-scales and actively incorporating supplementary control reserve capacity from time-variant sources.

X. Outlook

There are several directions for further research activity.

First of all extending the applicability of the ancillary service manager scheme towards the short-term incorporation of supplementary control reserve capacities from variable RES in-feed. Day-ahead electricity in-feed forecasts for wind and PV power can be used as a basis for estimating the available control reserve power coming from these sources. Stochastic MPC could be a suitable tool to handle forecast errors [44], [45].

Second, a stringent decision framework is needed for choosing the optimal control actuator for a given fault occurrence out of a given portfolio of different available control actuators, i.e using generator units versus using storage units or the curtailment of RES generation to tackle the fault.

Third, from the perspective of the ancillary service manager's MPC setup, there is a strong motivation for incorporating stability constraints, such as terminal cost terms in the form of so-called control Lyapunov functions (CLF) [22] or passivity-based functions [25], [26]. Such stability constraints guarantee the stability of the closed-loop MPC scheme, assuming that the MPC' model-plant mismatch is not decisive, and can provide a better and smoother grid control performance.

Furthermore, the problem of tackling the rapidly increasing computational effort for more complex networks and the necessary information exchange rests. The successful implementation of various decentralised MPC schemes for grid frequency control, such as cooperative-based DMPC schemes, have been presented [42].

Finally, the development of a unified grid control scheme that can act as an alternative for existing primary and secondary control schemes is envisioned.

Acknowledgement

The authors would like to thank Tobias Rinke, currently pursuing his master thesis at the ETH Power System Laboratory, for adapting an existing IEEE 14 bus benchmark system [46] for its usage with MPC schemes in Matlab/Simulink.

References

[1] M. Trotignon Y. G. Rebours, D. S. Kirschen and S. Rossignol. A survey of frequency and voltage control ancillary services part I: Technical features. *IEEE TRANSACTIONS ON POWER SYSTEMS*, VOL. 22, NO. 1, 2007.

[2] S. L. Andersson, A. K. Elofsson, M. D. Galus, L. Göransson, S. Karlsson, F. Johnsson, and G. Andersson. Plug-in hybrid electric vehicles as regulating power providers: Case studies of Sweden and Germany. *Energy Policy*, 38:2751–2762, 2010.

[3] Casey Quinn, Daniel Zimmerle, and Thomas H. Bradley. The effect of communication architecture on the availability, reliability, and economics of plug-in hybrid electric vehicle-to-grid ancillary services. *Journal of Power Sources*, In Press, Corrected Proof, 2009.

[4] M. D. Galus, R. La Fauci, and G. Andersson. Investigating PHEV wind balancing capabilities using heuristics and model predictive control. In *IEEE Power and Energy Society (PES) General Meeting*, Minneapolis, Minnesota, USA, 2010.

[5] M. D. Galus and G. Andersson. Power system considerations of plug-in hybrid electric vehicles based on a multi energy carrier model. In *Power and Energy Society (PES) General Meeting*, Calgary, Canada, 2009.

[6] M.D. Galus, M. Zima, and G. Andersson. On integration of plug-in hybrid electric vehicles into existing power system structures. *accepted to Energy Policy*, 2010.

[7] ENTSO-E. Continental europe operation handbook. *www.entsoe.eu*, 2004.

[8] EcoGrid. Steps toward a danish power system with 50% wind energy. *ECOGRID WP4: New measures for integration of large-scale renewable energy*, page 219, 2009.

[9] EU Decision No 406/2009/EC. *http://eur-lex.europa.eu/LexUriServ/LexUriServ.do?uri=OJ:L:2009:140:0136:01:EN:HTML*, 23 April 2009.

[10] US Department of Energy (DOE) States with Renewable Portfolio Standards. *http://apps1.eere.energy.gov/states/maps/renewable_portfolio_states.cfm*, accessed 15 June 2010.

[11] International Energy Agency (IEA). Deploying renewables. 2008.

[12] E. Santacana, G. Rackliffe, L. Tang, and X. Feng. Getting smart. *IEEE Power & Energy*, 8(2):41–48, March/April 2010.

[13] M.D. Galus, S. Koch, and G. Andersson. Provision of load frequancy control by phevs, controllabel loads and a co-generation unit. *submitted to IEEE Transactions on Industrial Electronics, Special Issue on Smart Grids*, 2010.

[14] Le Xie and Marija D. Ilić. Model predictive economic/environmental dispatch of power systems with intermittent resources. In *Power and Energy Society (PES) General Meeting*, Calgary, Canada, 2009.

[15] swissgrid Prequalification of Ancillary Services. *www.swissgrid.ch/power_market/grid_operation/ancillary_services/prequalification*, accessed 15 June 2010.

[16] B. Ernst, B. Oakleaf, M. Ahlstrom, M. Lange, C. Moerhlen, B. Lange, U. Focken, and K. Rohrig. Predicting the wind. *IEEE Power & Energy*, 5(6):78–89, December 2007.

[17] B. Ernst, F. Reyer, and J. Vanzetta. Wind power and photovoltaic prediction tools for balancing and grid operation. In *Integration of Wide-Scale Renewable Resources Into the Power Delivery System, 2009 CIGRE/IEEE PES Joint Symposium*, pages 1–9, 29-31 2009.

[18] G. Kariniotakis, I.H.-P. Waldl, I. Marti, G. Giebel, T. Nielsen, J. Tambke, J. Usaola, F. Dierich, A. Bocquet, and S. Virlot. Next generation forecasting tools for the optimal management of wind generation. In *9th International Conference on Probabilistic Methods Applied to Power Systems*, Stockholm, Sweden, 2006.

[19] swissgrid Weekly Tenders of Ancillary Services. *www.swissgrid.ch/power_market/grid_operation/ancillary_services/tenders/list/T100111_weekly-tender-schedule.pdf/en*, accessed 15 June 2010.

[20] C. V. Rao D. Q. Mayne, J. B. Rawlings and P. O. M. Scokaert. Constrained model predictive control: Stability and optimality. *Automatica*, 36(6):789-814, 2000.

[21] M. Morari and J. H. Lee. Model predictive control: Past, present and future. *Computers and Chemical Engineering*, 25:667–682, 1999.

[22] A. Jadbabaie. Nonlinear receding horizon control: a control lyapunov function approach. *Ph.D. Thesis, CDS Caltech*, 2000.

[23] J. A. Primbs. Nonlinear optimal two-dimensional nonlinear system control: a receding horizon approach. *Ph.D. Thesis, CDS Caltech*, 1999.

[24] H. Chen and F. Allgöwer. A quasi-infinite horizon nonlinear model predictive control scheme with guaranteed stability. *Automatica*, 34(10):1205–1218, 1998.

[25] C. Ebenbauer Raff, T. and F. Allgöwer. Nonlinear model predictive control: A passivity-based approach. In *International Workshop on Assessment and Future Directions of Nonlinear Model Predictive Control*, 2005.

[26] T. Raff Ebenbauer, C. and F. Allgöwer. Dissipation inequalities in systems theory: An introduction and recent results. *In R. Jeltsch and G. Wanner, editors, Invited Lectures of the International Congress on Industrial and Applied Mathematics 2007*, pages 23–42, 2009.

[27] E. D. Sontag. Nonlinear regulation: The piecewise linear approach. *IEEE Transactions on Automatic Control*, 26(2):346–358, 1981.

[28] F. Borrelli Bemporad, A. and M. Morari. Explicit solution of lp-based model predictive control. In *Proc. 39th IEEE Conf. on Decision and Control*, Sydney, Australia, 2000.

[29] M. Morari V. Dua Bemporad, A. and E. N. Pistikopoulos. The explicit linear quadratic regulator for constrained systems. *Automatica*, 38(1):3–20, 2002.

[30] M. Baotić A. Bemporad Borrelli, F. and M. Morari. Dynamic programming for constrained optimal control of discrete-time hybrid systems. *Automatica*, 41:1709–1721, 2005.

[31] F. Borrelli. Constrained optimal control of linear and hybrid systems. *Lecture Notes in Control and Information Sciences*, 290, 2004.

[32] A. Bemporad and C.Filippi. Suboptimal explicit rhc via approximate multiparametric quadratic programming. *Technical Report, ETH Zurich*, AUT02-07, 2002.

[33] G. Andersson. Dynamics and control of electric power systems. *Lecture Script, EEH–Power Systems Laboratory, ETH Zurich*, 2010.

[34] M. Geidl and G. Andersson. Optimal power flow of multiple energy carriers. *IEEE Transactions on Power Systems*, 22(1):145–155.

[35] US EPA. Dynamometer driver's aid, testing and measurement. Available on: http://www.epa.gov/otaq/emisslab/testing/dynamometer.htm#vehcycles, accessed 17th August 2007.

[36] M. D. Galus and G. Andersson. Demand management for grid connected plug-in hybrid electric vehicles (phev). In *IEEE Energy 2030*, pages 1–8, Atlanta, GA, USA, 2008.

[37] M. D. Galus and G. Andersson. Integration of plug-in hybrid electric vehicles into energy systems. In *Powertech 09*, Bucharest, Romania, 2009.

[38] P. M. Anderson and A. A. Fouad. Power system control and stability. *IEEE Press*, 1994.

[39] A. J. Wood and B. F. Wollenberg. Power generation, operation and control 2nd ed. *Wiley, New York*, 1996.

[40] P. Grieder Baotić M. Kvasnica, M. and F. J. Christophersen. Multi-parametric toolbox (MPT). *http://control.ee.ethz.ch/~mpt/"*, 2006.

[41] S. Koch, M. Zima, and G. Andersson. Active coordination of thermal household appliances for load management purposes. In *IFAC Symposium on Power Plants and Power Systems Control*, Tampere, Finland, 2009.

[42] I. A. Hiskens J. B. Rawlings Venkat, A. N. and S. J. Wright. Distributed mpc strategies with application to power system automatic generation control. *IEEE Transactions on Control Systems Technology*, 6(6):1192–1206, 2008.

[43] E. Camponogara, D. Jia, B. H. Krogh, and S. Talukdar. Distributed model predictive control. *IEEE Control Systems Magazine*, 22(1):44–52, Feb. 2002.

[44] J. A. Primbs and C. H. Sung. Stochastic receding horizon control of constrained linear systems with state and control multiplicative noise. *IEEE Transactions on Automatic Control*, 2008.

[45] D. Chatterjee Hokayem, P. and J. Lygeros. On stochastic receding horizon control with bounded control inputs. In *IEEE Conference on Decision and Control*, 2009.

[46] L. Friedrich and M. Gautschi. Grid stabilization control and frequency regulation for inverter-connected distributed renewable energy sources. *Master Thesis, University of Wisconsin, Madison (Dept. of Elektrical & Computer Engineering) & ETH Zurich (EEH–Power Systems Laboratory)*, 2009.